

REPORT DOCUMENTATION PAGE

Form Approved
OMB No. 0704-0188

Public reporting burden for this collection of information is estimated to average 1 hour per response, including the time for reviewing instructions, searching existing data sources, gathering and maintaining the data needed, and completing and reviewing this collection of information. Send comments regarding this burden estimate or any other aspect of this collection of information, including suggestions for reducing this burden to Department of Defense, Washington Headquarters Services, Directorate for Information Operations and Reports (0704-0188), 1215 Jefferson Davis Highway, Suite 1204, Arlington, VA 22202-4302. Respondents should be aware that notwithstanding any other provision of law, no person shall be subject to any penalty for failing to comply with a collection of information if it does not display a currently valid OMB control number. **PLEASE DO NOT RETURN YOUR FORM TO THE ABOVE ADDRESS.**

1. REPORT DATE (DD-MM-YYYY) 01-12-2011		2. REPORT TYPE Final Technical Report		3. DATES COVERED (From - To) 05-01-2007 to 10-31-2010	
4. TITLE AND SUBTITLE Ceramics for High Power Lasers				5a. CONTRACT NUMBER	
				5b. GRANT NUMBER FA9550-07-1-0392	
				5c. PROGRAM ELEMENT NUMBER	
6. AUTHOR(S) R.L. Byer, R.M. Gaume, R.K. Route, Y. He				5d. PROJECT NUMBER	
				5e. TASK NUMBER	
				5f. WORK UNIT NUMBER	
7. PERFORMING ORGANIZATION NAME(S) AND ADDRESS(ES) Edward L. Ginzton Laboratory Stanford University Stanford, CA 94305-4088				8. PERFORMING ORGANIZATION REPORT NUMBER SPO No. 39048	
9. SPONSORING / MONITORING AGENCY NAME(S) AND ADDRESS(ES) AFOSR 801 North Randolph Street, Room 732 Arlington, VA 22203-1977				10. SPONSOR/MONITOR'S ACRONYM(S)	
				11. SPONSOR/MONITOR'S REPORT NUMBER(S) AFRL-OSR-VA-TR-2012-0622	
12. DISTRIBUTION / AVAILABILITY STATEMENT Approved for public release; distribution unlimited.					
13. SUPPLEMENTARY NOTES The view, opinions and/or findings contained herein are those of the author(s) and should not be construed as necessarily representing the official policies or endorsements, either expressed or implied, of the Air Force Office of Scientific Research or the U.S. Government.					
14. ABSTRACT Transparent ceramic gain-media can lead, when properly engineered, to significant improvements in solid-state laser performance. Amongst the anticipated benefits of such material-based lasers are high-average power outputs with higher efficiencies, improved pulse-energy storage and outputs, higher ultrafast-laser performance, and phased-array operation of guided-wave laser systems. In this research program we focus on the application, design and testing of engineered laser ceramics. We are working on (1) the characterization of the lasing performance of composite laser ceramics, (2) strategies for evolving composites to achieve high laser efficiency and (3) the design of novel ceramic composites to reduce parasitic losses during operation. We hope that the dual focus on correlating processing, performance and optical losses will lead to exceptional quality ceramics and a fundamental understanding about these materials at all levels of manufacturing and use. Dr. A. Ikesue of JFCC is our major international partner, with funding derived through AFOSR/AOARD. The synergy between Stanford and JFCC is accelerating progress in the implementation of these materials in high-power laser applications.					
15. SUBJECT TERMS Ceramic laser, high energy laser, transparent ceramics, engineered ceramics, transparent polycrystalline material					
16. SECURITY CLASSIFICATION OF:			17. LIMITATION OF ABSTRACT	18. NUMBER OF PAGES	19a. NAME OF RESPONSIBLE PERSON Robert L. Byer
a. REPORT	b. ABSTRACT	c. THIS PAGE			19b. TELEPHONE NUMBER (include area code) (650) 723-0226
				29	

SF 298 Continuation Sheet
Interim Technical Report, Cont.

1. AFOSR GRANT NUMBER: FA9550-07-1-0392
2. PERIOD COVERED BY REPORT: 05-01-2007 to 10-31-2010
3. TITLE OF PROPOSAL: Ceramics for High Power Lasers
4. LIST OF MANUSCRIPTS SUBMITTED OR PUBLISHED UNDER AFOSR SPONSORSHIP DURING THIS REPORTING PERIOD:

A.P. Patel, M.R. Levy, R.W. Grimes, R.M. Gaume, R.S. Feigelson, K.J. McClellan, and C.R. Stanek, "Mechanisms of non-stoichiometry in $Y_3Al_5O_{12}$ ", Applied Physics Letters, **93**, 191902 (2008)

J.A. Wisdom, R. Gaume and R.L. Byer, "Confocal laser-gain scanning microscopy: a new imaging technique for engineered laser-gain media", submitted.

J.A. Wisdom, R. M. Gaume, K. Urbanek, T. Plettner, R.L. Byer, A. Guichard, M.Brongersma, A. Kinkhabwala, W.E. Moerner, Akio Ikesue, Yan Lin Aung, "Characterization of a Nd:YAG Ceramic Laser with a 510- μ m-wide Engineered Doping Profile", submitted.

5. SCIENTIFIC PERSONNEL SUPPORTED BY THIS PROJECT AND DEGREES AWARDED DURING THIS REPORTING PERIOD:

Faculty - R. L. Byer
Staff - R. M. Gaume, R.K. Route
Graduate Student - Y. He

6. REPORT OF INVENTIONS BY TITLE ONLY:
7. SCIENTIFIC PROGRESS AND ACCOMPLISHMENTS: See Interim Technical Report
8. TECHNOLOGY TRANSFER:

This program explores micro-structured ceramic materials for use as transparent laser host materials to replace crystalline laser host materials. Technology developed under this program will be available through Stanford's Office of Technology and Licensing.

9. CORRESPONDENCE ADDRESS:

Robert L. Byer, P.I.
Ginzton Laboratory, Mail Code 4088 (tel) 650-723-0226
Stanford University (fax) 650-723-2666
Stanford, CA 94305-4088 byer@stanford.edu

Table of Contents

I.	Introduction	5
II.	Technical Report	5
III.	Directions for Continuing Research	28
IV.	Program Participants	29
V.	Publications Supported Directly	29

I. Introduction

The present document constitutes the final report of our 42-month research program on ceramics for high-power lasers. The objectives of this program, under AFOSR support FA9550-07-1-0392 (04/23/07 - 10/31/10) were the following:

- 1) Study the fabrication of laser-grade transparent ceramics as well as the possibilities and limitations that ceramic microstructure places on engineered doping profiles,
- 2) Study the optical quality and size scalability (up to several cm) of diffusion-bonded materials such as YAG and Y_2O_3 for use as Talbot-imaged planar waveguides
- 3) Study grain-boundary diffusion using optical methods to determine what dopant profile shapes can be fabricated

II. Technical Report

1. Proposed research program

Our objective was to establish a fundamental understanding of how ceramic YAG laser host can be designed to yield laser components with superior laser performance. Using expertise in transparent ceramics fabrication, micro-scale optical characterizations, laser design and laser testing, we sought to advance the fundamental knowledge about engineered gain media for high-power laser materials.

In particular, we were interested in designing test structures for improved laser efficiency at high-power and developing algorithms to solve the inverse diffusion problem for creating desired dopant concentration profiles. We primarily focused on parabolic and hyperbolic dopant concentration profiles in transparent optical ceramics. This work necessitated an in-depth understanding of dopant diffusion to control gain and loss in engineered gain-media and required the development of specific ceramic processing methodologies to achieve precise spatial control of dopants in the host.

2. Accomplishments

2.1 Progress on the fabrication of ceramic YAG gain media

During this program, we have produced laser grade Nd:YAG and low optical loss Gd^{3+} doped YAG and Tm:YAG ceramics. Laser performance is still currently limited by residual scattering in our ceramic Nd:YAG.

We have carried out comparative studies on different YAG powders and powder forming techniques. These investigations were followed by the fabrication of transparent YAG ceramics by vacuum sintering. This work soon motivated a specific study on the influence of chemical composition on the fabrication of transparent ceramics. This approach not only helped us to obtain better consistency in our fabrication process but also led to new developments in the role played by point defects in non-stoichiometric YAG.

Mass loss upon calcination in the starting powders is the main contributor to departure from stoichiometric composition. A series of YAG ceramic samples with compositions varying around stoichiometry within $\pm 1\text{mol}\%$ was prepared (Fig. 1) and this helped us in determining the solubility limit of both alumina and yttria excess in the YAG phase. The distortion of the YAG lattice parameter induced by the solute in excess was measured by XRD and compared with optical micrograph and scattering data (Fig. 2). These characterizations have shown that at most 0.1 mol% of alumina and 0.2 mol% of yttria were soluble in YAG when typical cooling rates ($>600^\circ\text{C}/\text{hr}$) are used.

In a joint work with Los Alamos National Laboratory and Imperial College in London [1], we have been able to relate these lattice parameter changes to the actual nature of the point defects that form as a consequence of composition departure from stoichiometry. It has already been proven that these defects have a profound effect on diffusion kinetics and therefore on densification, grain-growth and dopant diffusion. In addition, they may also affect optical performance by introducing color centers that will compete with normal laser operation or favor photo-darkening. Contrary to crystal growth, transparent ceramics processing allows for fine composition tuning that is not dictated by thermodynamic equilibria at the liquidus. This particular aspect was a key concept to enable the present investigation. This study not only validates the computational tools that our collaborators developed to model non-stoichiometry in a crystalline lattice, but it also shed a new light on defect formation energetics in the YAG crystalline structure. This work is currently being continued in an attempt to identify the nature and the depth of traps in the band gap. We have recently performed thermally stimulated luminescence (TSL) measurements in the same series of YAG samples in collaboration with Dr. A. Vedda at the University of Milano-Bicocca. Our results clearly show specific features in the intensity of the TSL glow curve which strongly depends on Y_2O_3 concentration across the series of ceramic samples. Similar TSL peak positions between the ceramics and undoped crystal grown by the Czochralski method (Fig. 3) confirm the intrinsic nature of these traps (not due to impurities). We are now undertaking more detailed analyses to relate this work to the modeling work done earlier.



Fig. 1 Series of YAG ceramic samples (4-mm thick) made at Stanford with compositions varying by slight increments of Al_2O_3 or Y_2O_3 near stoichiometric composition. Samples on the left side are $\text{Nd}^{3+}:\text{YAG}$ (pink), while samples on the right are $\text{Gd}^{3+}:\text{YAG}$ (yellowish). The cloudiness of the samples is associated with the presence of remaining porosity and secondary phases.

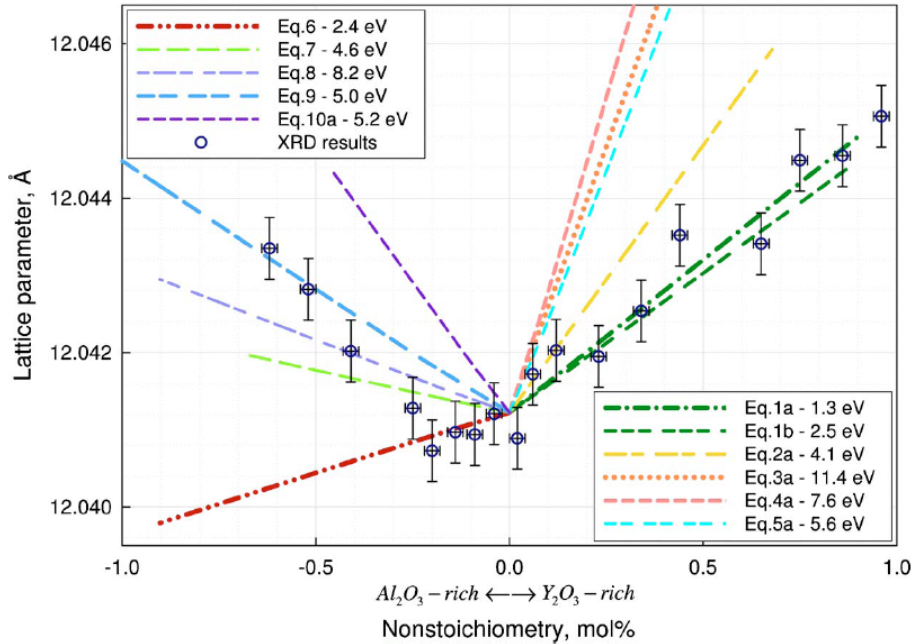


Fig. 2 The variation in YAG lattice parameter with respect to deviations from stoichiometry, determined by either atomistic simulation or XRD. The simulation results correspond to various defect reactions identified in this work.

Besides the benefits that this fundamental study will provide on the general understanding of laser ceramic fabrication and performance, it is also expected that it will impact the field of scintillator ceramics.

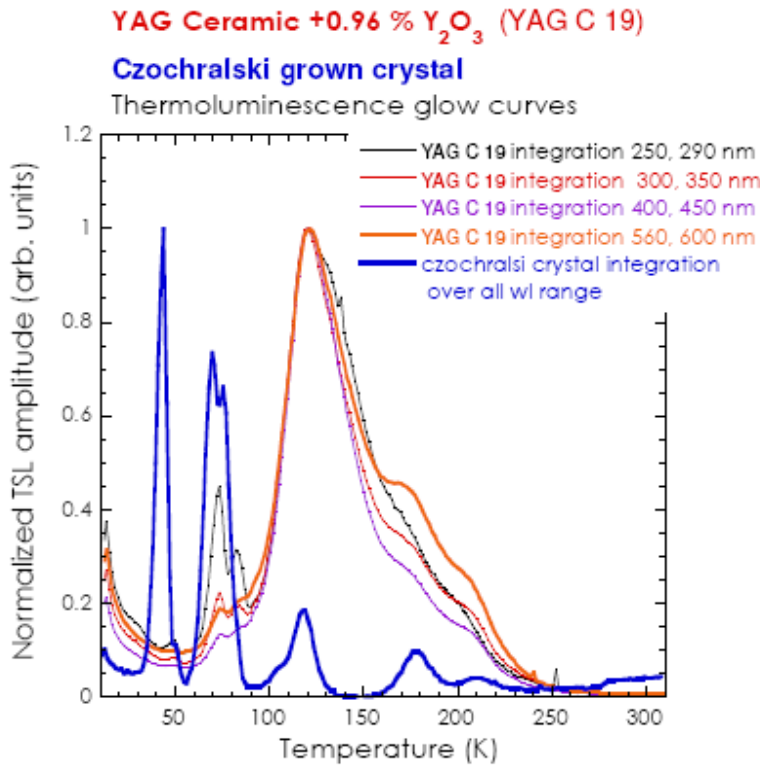


Fig. 3 Comparison between the thermally stimulated luminescence (TSL) spectra of a heavily Y-doped YAG ceramic made at Stanford and of an undoped single-crystal (blue curve). The comparable position of the peaks in both samples confirms the intrinsic nature of traps. Note the large concentration of deep traps in the ceramic (broad peak corresponding to the de-trapping of electrons at higher temperatures ~ 120 K).

2.2 Effect of ceramic composition on transparency

The phase diagram of Al_2O_3 - Y_2O_3 mixtures indicates that the secondary phases formed in non-stoichiometric YAG are alumina in case of an excess of Al_2O_3 and YAlO_3 (YAP) in the case of an excess of yttria. Because pores, Al_2O_3 and YAP have different indices of refraction with respect to YAG, their presence will reduce the transparency of YAG ceramic samples [2]. To understand the effect of composition on the formation of scatters, we used a Mie scattering model to fit the transmittance spectra of these non-stoichiometric samples. The ceramic samples prepared for these studies were obtained by reactive sintering using the same amount of sintering aid (0.5 wt % TEOS) and without luminescent ion doping.

Assuming all scatters are spherical, we found that a bi-modal distribution of sizes was necessary to reproduce by modeling the observed transmission spectra. For samples with an excess of Al_2O_3 (negative departure from stoichiometry in the figures below), we considered two types of scatters: those formed of pores and those formed of Al_2O_3 . Conversely, for samples with an excess of Y_2O_3 (positive departure from stoichiometry in the figures below), those formed of pores and those formed of YAP were considered. Adopting the Sellmeier equations for YAG [3], Al_2O_3 [4] and YAP [5] for index dispersion, four parameters were fitted to match the transmission spectra of the various ceramic samples, namely the volume fractions V_{p1} and V_{p2} and sizes r_1 and r_2 of pores and precipitates, respectively. Errors on each parameter value have been calculated in order to estimate the accuracy of our fitting procedure. The volume fraction of solid precipitates V_{p2} as a function of the ceramic composition is presented on Fig. 4. The V_{p2} values follow quite nicely the expected volume excess of Al_2O_3 and YAP with respect to the YAG composition. For the two compositions near stoichiometry however (0 and 0.05 mol% of Y_2O_3), the values of V_{p2} obtained from Mie's model do not seem to follow this expected trend. Reasons for this discrepancy are still under investigation but might originate from the fact that our model is not accounting for the scattering of silicate-based precipitates, which might have formed at the grain boundaries if the cooling rate of the ceramics was too slow. The evolution of the porosity and ceramic density with stoichiometry derived from Mie's modeling is shown on Fig. 5 (left). As expected, the pore density reaches a minimum for the stoichiometric composition, on the order of $3.8 \times 10^5 \text{ cm}^{-3}$ in the ceramics produced for this study (Fig. 5. right). This number compares with those measured by the Laser Scattering Tomography (LST) in similar reactively sintered YAG ceramic samples obtained from Japan (section 2.4.4, table 3). In addition, the size of the secondary phases measured by high-resolution optical microscopy confirms the values obtained through our fitting method (Fig. 6). While agglomerated Al_2O_3 precipitates are easily identified in Al_2O_3 -rich samples, small-sized YAP precipitates ($<0.1 \mu\text{m}$) appear finely divided in Y_2O_3 -rich samples.

This modeling suggests that the effective composition window leading to high transparency in ceramics (no secondary phases AND no porosity) is narrower than the solid-solution domain determined from lattice cell distortion through XRD analysis (see paragraph 2.1). This may be due to sluggish kinetics in the solubility equilibrium process existing between Al_2O_3 and Y_2O_3 and the YAG phase as the system approaches stoichiometry.

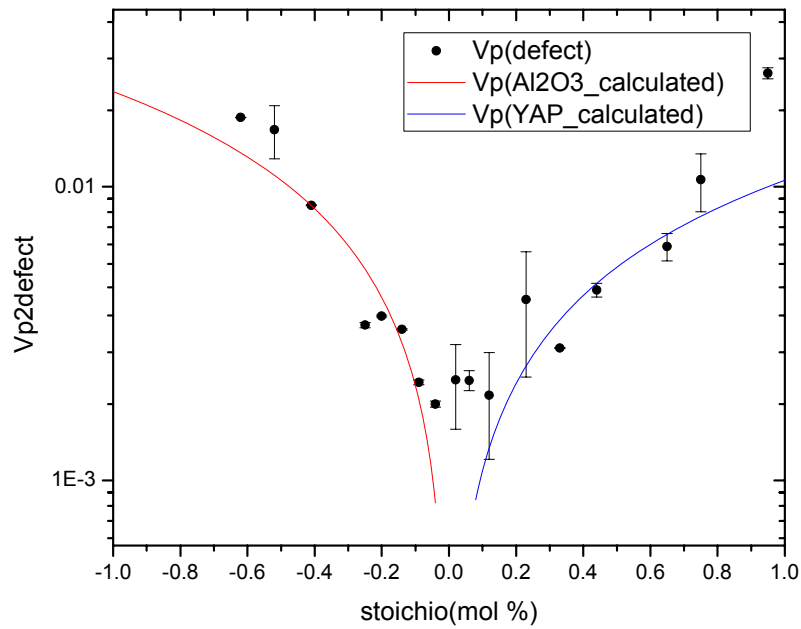


Fig. 4 Volume fraction of solid precipitates as a function of stoichiometry in YAG ceramics where the x-axis represents the excess of yttrium relative to the stoichiometric YAG composition. The red curve represents the expected volume fraction of precipitated alumina and the blue curve that of precipitates of YAP, calculated from the initial composition.

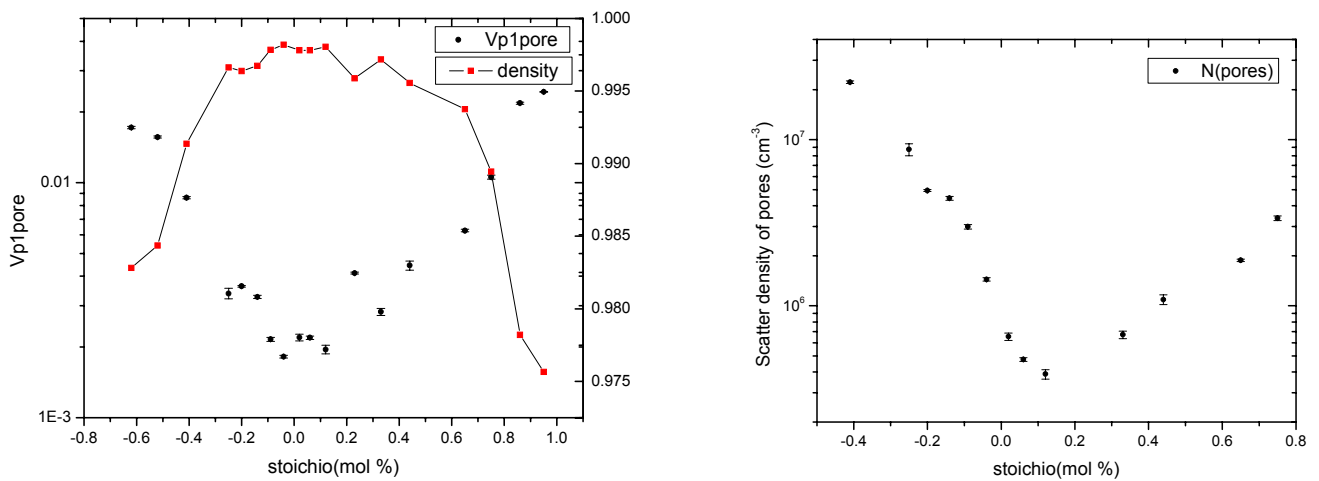


Fig. 5 Evolution of the volume fraction of pores and ceramic density with stoichiometry (left) and evolution of the pore density as a function of stoichiometry in YAG ceramics (right). The x-axis represents the excess of yttrium relative to the stoichiometric YAG composition.

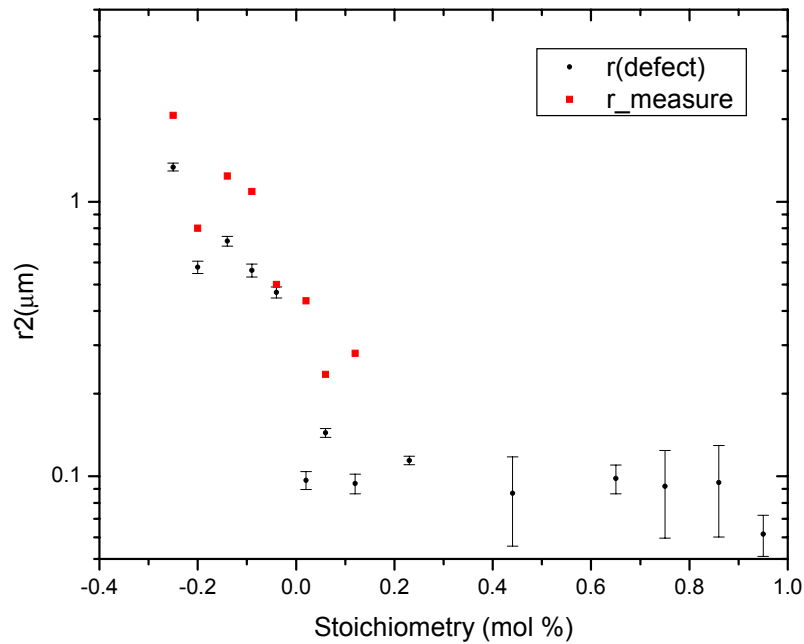


Fig. 6 Evolution of size of secondary phases (Al_2O_3 and YAP) as a function of stoichiometry in YAG ceramics, determined from modeling and microscopy measurements. The X-axis represents the excess of yttrium relative to the stoichiometric YAG composition.

- [1] A.P. Patel, M.R. Levy, R.W. Grimes, R.M. Gaume, R.S. Feigelson, K.J. McClellan, and C.R. Stanek, “Mechanisms of non-stoichiometry in $\text{Y}_3\text{Al}_5\text{O}_{12}$ ”, Applied Physics Letters, **93**, 191902 (2008)
- [2] I. Sakaguchi et al., *J. Am. Ceram. Soc.* **79** (1996), 1627
- [3] <http://www.vloc.com/PDFs/YAGBrochure.pdf>
- [4] J.F. Shackelford, R.H. Doremus, “Ceramic and Glass Materials: Structure, Properties and Processing”, Google eBook, p 21-22
- [5] Z. Zeng et al, “Measurement of the refractive index and thermal refractive index coefficients of Nd:YAP crystal”, Appl. Opt., **29**(9), 1281-1286 (1990)

2.3 Progress on the design of engineered ceramic gain media

The results from our investigations into micro-engineered ceramic structures provided several critical insights. First, the length scale of possible doping profiles can be characterized by measuring distance over which the doping level falls to $1/e$ its initial value, referred to as L , the diffusion length. Multiplying this distance by two is a measure of the possible width of engineerable doping profiles. Accordingly, the measurements of Nd-diffusion distance in reactively sintered ceramics demonstrate that the smallest width for state-of-the-art reactive-sintering techniques is 500 microns wide. The next two questions to ask are what materials systems and processing conditions are best suited for much smaller profile widths (~ 10 microns), and, how useful are large profiles for laser performance.

2.3.1 Processing conditions for 10 μm-wide doping profiles

There are tradeoffs between sintering time and temperature on the overall transparency of a ceramics and the distance doping ions are expected to travel. If a ceramic is sintered at a low temperature for a short time, for example, the dopant ions are not expected to travel very far. However, the optical quality of the ceramic can be expected to suffer because at low temperatures and times the pores within the ceramic are not able to collapse, leaving scattering centers. We performed measurements of the diffusion distances of Nd ions in fully densified (transparent) ceramics and for different sintering times and temperatures. This allowed us to determine the maximum processing time and temperature for 10 μm -wide profiles.

The variation of the diffusion length with sintering time, t , and sintering temperature T , was experimentally shown to follow,

$$L = \frac{t^{3/10}}{\exp(E/(RT) - A)},$$

where E is an experimentally determined activation energy with a value of 310 +/- 30 kJ/mol, R is the ideal gas constant and A is a constant with a value of 21.92 using units of microns/hour. According to the measurements, if the initial nanoparticles are larger than 200 nm, 10-micon-wide doping profiles can be fabricated by sintering at 1650°C, for up to 200 hours. There is a greater potential for small doping profiles with single-phase sintering techniques, rather than reactive sintering.

2.3.2 Centimeter-scale doping profiles for laser applications

Doping profiles with 1-cm-and-larger widths are readily achievable with current ceramic processing techniques. One application for doping profiles is to simplify edge pumping of slab lasers by clustering more dopant in the center of the gain medium where it can be easily extracted by a TEM₀₀. The figure below shows the relevant geometry. For standard edge-pumped lasers, a gain medium with a uniform doping profile is used. This results in power being absorbed at the edges of the gain medium making it difficult to extract. Clustering more dopant in the center of the slab allows the slab to operate more efficiently with TEM₀₀ beams.

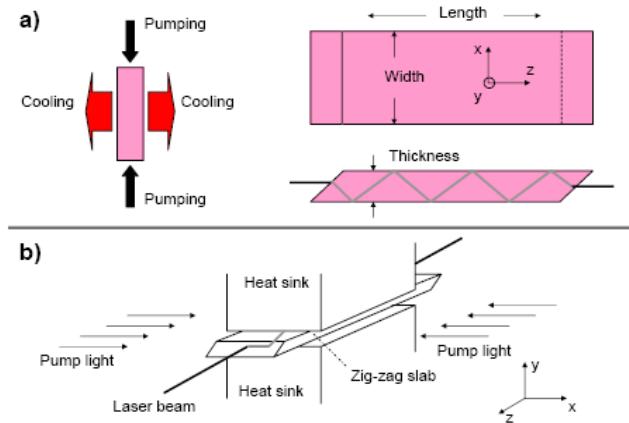


Fig. 7 End-pumped (top) and edge-pumped (bottom) geometries

There is a complication that comes with changing the doping level of gain ions: as the doping level is varied the refractive index also changes. Refractive index variations from doping profiles can distort TEM₀₀ beams, eliminating the advantage of more efficient pumping and extraction. Therefore, the doping profile used must be carefully considered, so that it both improves extraction but does not result in large beam distortions. Using a genetic algorithm, we determined a doping profile that was able to improve wall-plug efficiency for an edge-pumped Nd:YAG slab by 39% over an optimally designed uniformly doped slab. The resulting profile is shown below.

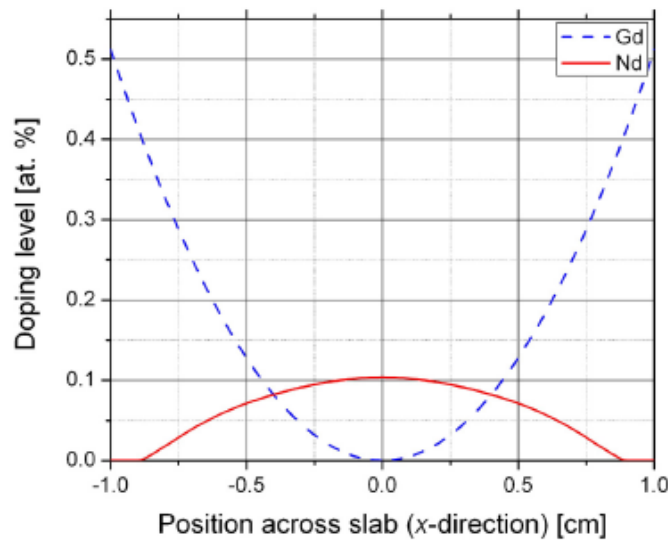


Fig. 8 Calculated Nd³⁺ and Gd³⁺ doping concentrations in the cross-section of a laser slab optimized for edge-pumping operation.

We have produced ceramic composites (Fig.9) at Stanford with simple Nd³⁺ and Gd³⁺ profiles and have been carrying optical characterizations. Laser-scanning confocal microscopy was used to measure the spatial distribution of Nd³⁺ ions by fluorescence detection. Confocal microscopes offer high spatial resolution as laser wavelength by combining a tightly focused laser beam with a confocal imaging system. In Fig.10 (a), at each point, a fluorescence spectrum is recorded. The fluorescence intensity at 885nm considered to be 1% Nd doped and the darker point is 0%

Nd^{3+} doped. The scanning images in Fig. 10 (b), (c), (d), clearly show the larger diffusion of Nd^{3+} along grain boundaries than lattice. The doping profiles (Fig. 11) are calculated from maps in Fig.10 by taking the average intensity on sections parallel to the interface. The diffusion length of Nd^{3+} increases as heating time increases, limited to $20\mu\text{m}$ after 92hrs heating.

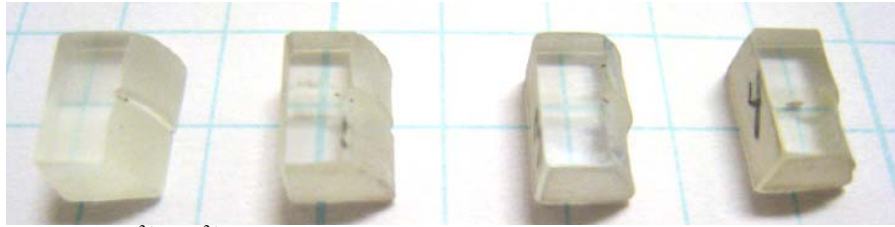


Fig. 9 Nd^{3+} , Gd^{3+} :YAG ceramic composites made at Stanford by thermal bonding. Samples are 7 mm long and are laser grade.

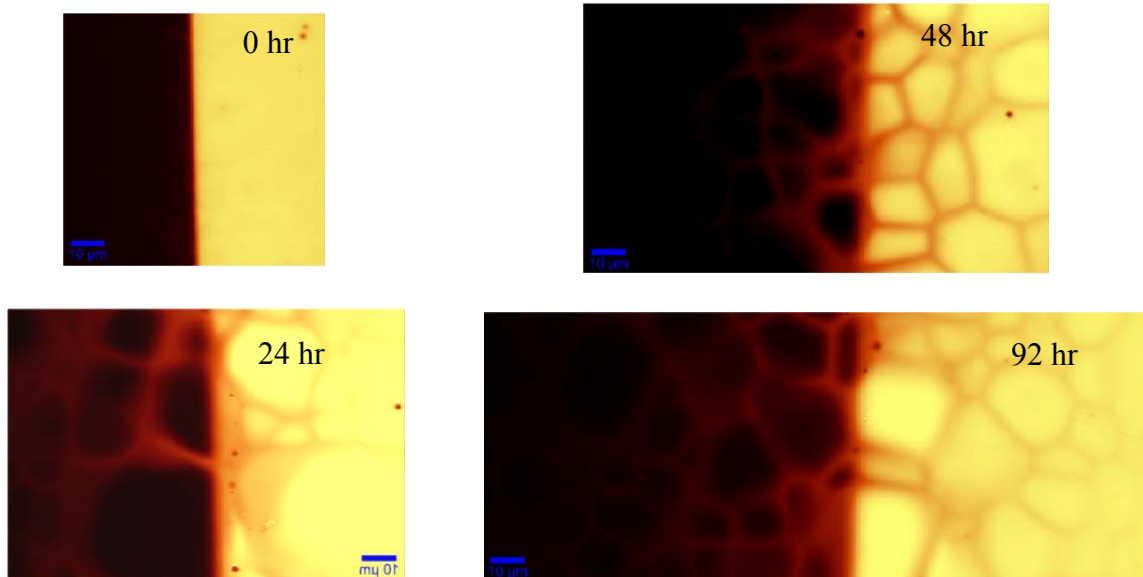


Fig. 10 Scanning confocal microscope spectroscopy images of bonded Nd:YAG (right side) and Gd:YAG (left side) annealed at 1700C for 0hr, 24hrs, 48hrs and 92hrs, respectively. (Scale bar = $10\mu\text{m}$)

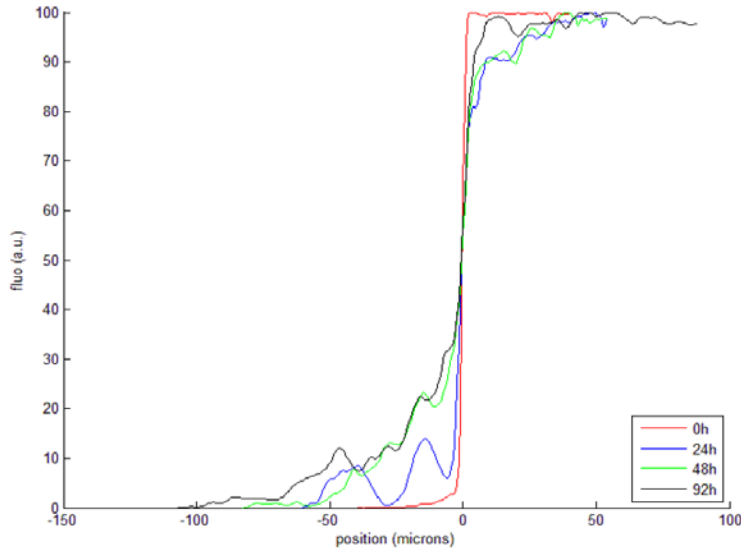


Fig. 11 Dopant profile of bonded Nd:YAG (right side) and Gd:YAG (left side) annealed at 1700C for 0hr, 24hrs, 48hrs and 92hrs.

In an attempt to verify that gadolinium doping can be used to compensate for the change of refractive index induced by the gradient of neodymium concentration, we have measured the wavefront distortion of a He-Ne laser beam (633nm) perpendicular to the bonded interface of a 1at% Nd:YAG||1at% Gd:YAG bonded ceramic sample. A wavefront sensor (Schack-Hartmann) was used for this measurement. The recorded phase is shown on Fig.12 and shows an average phase difference of around 10^{-7} across the bonded interface. This phase shift corresponds to an estimated value of 6×10^{-5} for the difference in refractive index between the two sides of the bond. This value compares reasonably well with the expected index difference $\Delta n \sim 3 \times 10^{-5}$ between Nd:YAG and Gd:YAG obtained from literature. These sensitive measurements will however need to be refined and confirmed in the future.

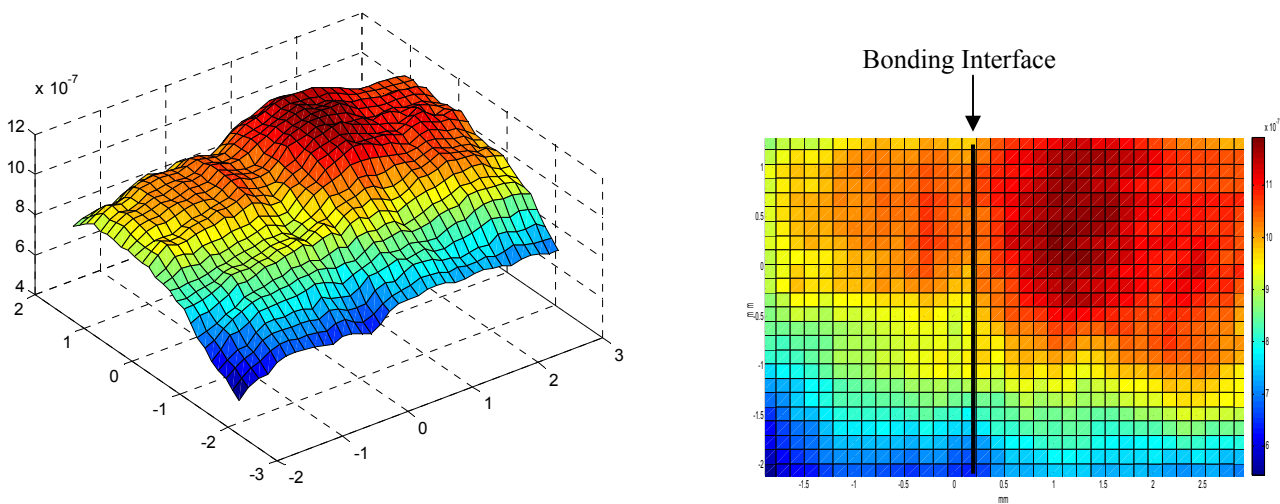


Fig. 12 Phase distortion of a planar laser wavefront propagating perpendicular to a bonded Nd:YAG||Gd:YAG interface.

2.4 Progress on the characterization of low-loss laser ceramics

We are also interested to develop adequate instrumentation to better evaluate optical losses in high quality transparent ceramics and provide guidance for improving the ceramic fabrication process. In the past period, we have characterized three ceramic slabs produced by Dr. A. Ikesue *et al.* at World-Lab. Co. Ltd. Nagoya, Japan. The slabs (6x10x75mm) were polished on all sides (Fig.13). In most instances, these samples have been compared with a 1 at% Nd:YAG single-crystal and a 1 at% Nd:YAG ceramic purchased from Scientific Materials and Konoshima Corp. respectively.

Table 1 Samples tested

Material	Origin	Sample reference #
Undoped YAG ceramic	Ikesue	Z-713
1 at% Nd:YAG ceramic	Ikesue	Z-714
1 at% Gd:YAG ceramic	Ikesue	Z-715
1 at% Nd:YAG ceramic	Konoshima	Kono1
1 at% Nd:YAG single crystal	Scientific Materials	Sc1

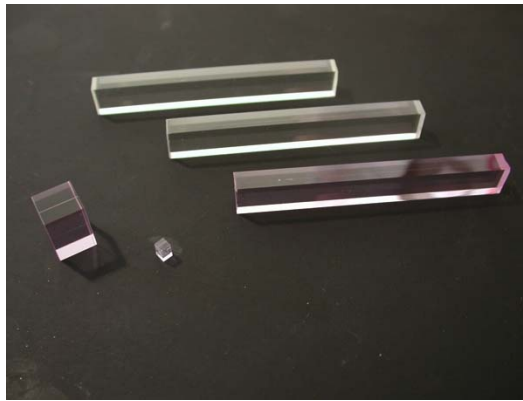


Fig. 13 Transparent ceramic slab of YAG, Nd³⁺:YAG and Gd³⁺:YAG. The Konoshima (10x10x20 mm) and single-crystal (3x3x5mm) test samples are on the left.

Absorption spectroscopy, thermalized absorption, light scattering tomography were used to quantify the absorption and scattering losses in all samples. In addition, confocal laser-gain scanning microscopy as well as laser tests were performed with Nd doped YAG ceramics.

2.4.1 Absorption Spectroscopy

The optical quality of ceramic samples was evaluated over a broad wavelength range. A Cary 500 spectrometer with double-beam transmission was used to measure the absorption coefficient in NIR-Vis-UV range (175-2000nm). The absorption coefficient α was calculated according to the equation:

$$\frac{I}{I_o} = 10^{-OD} = (1 - R)^2 \exp(-\alpha L) \quad (1)$$

Where I_0 and I are the intensities of the incident and transmitted light, O.D is the optical density measured by the spectrophotometer, R is the Fresnel reflection at normal incidence per interface, and L is the sample thickness.

We first verified that, in the Nd doped sample, the linear absorption coefficient at 808 nm was consistent with a 1 at% doping level. We also found that the absorption spectra of the undoped and Gd-doped YAG samples exhibit absorption peaks characteristic of a luminescent rare-earth contaminant (Fig 14). The superimposition of these spectra with the Z-714 one strongly suggests a neodymium contamination in these two other samples. This contamination likely originates from the ball-milling operation where the same jar has been used to process the various compositions.

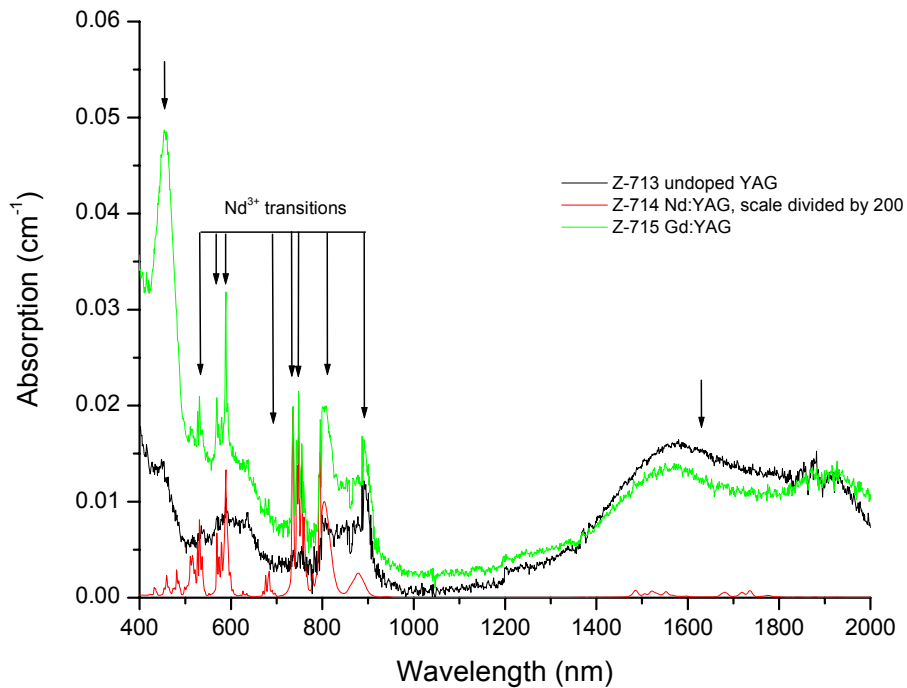


Fig. 14 Comparison of Z-713, Z-714, Z-715 absorption spectra in the absorption range of Nd^{3+} .

Based on linear absorption coefficient measurements, we estimate neodymium impurity levels to 30 ppm and 60 ppm in Z-713 and Z-715 respectively. In addition, three broad and intense absorption bands centered at 457 nm, 1550 and 1900 nm are observed in the undoped and Gd-doped samples. The latter two bands overlap with absorption lines of the ${}^4\text{I}_{9/2}-{}^2\text{I}_{15/2}$ transitions but are more intense and broader. This suggests a contamination by transition ions.

As a comparison, the absorption of Z-714 is plotted in Fig. 15 against the absorption of a Kono1 and Sc1. Z-714, SC1 and Kono1 all exhibit the same features in their absorption spectra. One can notice however that the absorption edge near band-gap ($\lambda < 300\text{nm}$) increases more dramatically in Z-714 than in the other two test samples. This attenuation is possibly due to light scattering from residual porosity.

The three ceramic slabs Z-71X present good optical quality with transmission values reaching the Fresnel limit. However, conventional absorption spectroscopy is not well suited to accurately measure low absorption levels. Therefore, we used the thermalized absorption technique to better quantify absorption losses in these samples.

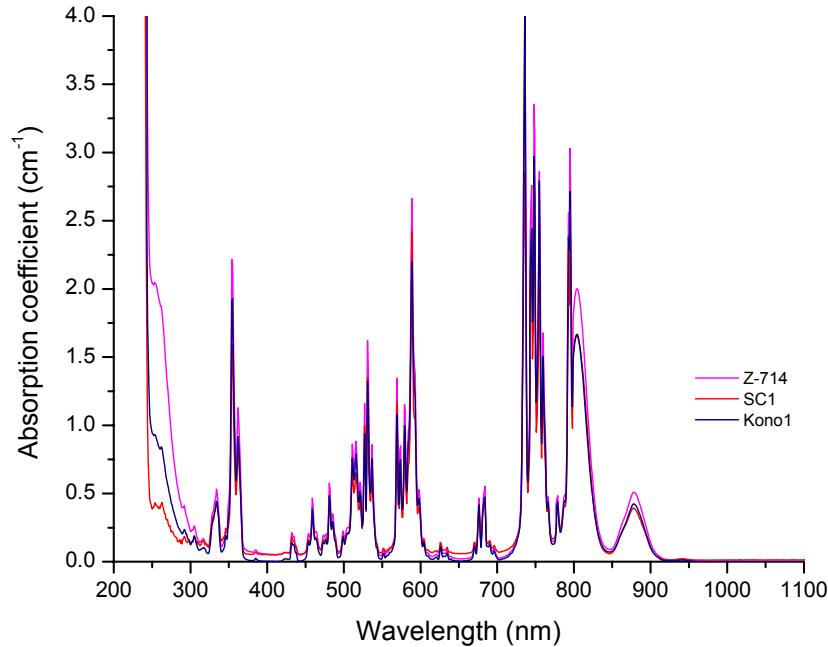


Fig. 15 Comparison of the absorption spectra of Z-714, Kono1, Sc1.

2.4.2 Thermalized absorption

Thermalized absorption measurements are made using a photothermal common-path interferometer (PCI). This method was developed at Stanford to measure low absorption levels in bulk optical materials. The principle of this technique is illustrated in Fig. 16. A powerful laser of wavelength λ is tightly focused on the sample. If the material is absorbing at this wavelength, heat will be generated and create a thermal lens. This lens is probed by interferometry using a second laser. The phase shift introduced by this lens is given by:

$$\Delta\phi = kL \frac{\partial n}{\partial T} \Delta T$$

Where k is the wavevector of the probe laser, L is the sample thickness, ΔT is the temperature increase induced by the pump laser, and $\partial n/\partial T$ is the thermo-optic coefficient of the material.

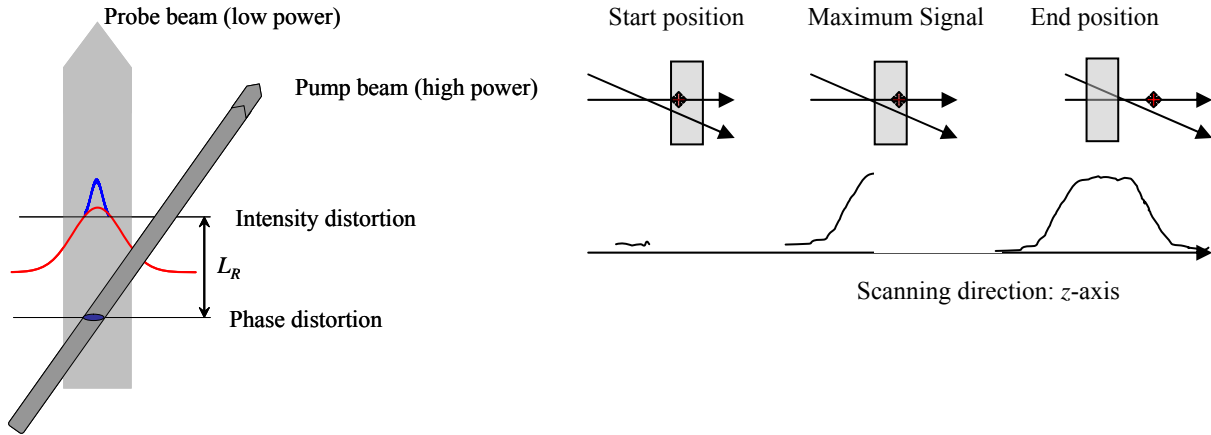


Fig. 16 PCI Method (left) and measurement technique (right)

Generally, this method can measure absorption levels down to 0.1 ppm/cm. In the present characterization studies, the absorption measurements were obtained at a pump wavelength of 1064 nm. The beam sizes of the probe and pump lasers were 240 μm and 70 μm respectively. Individual scattering defects smaller than 40 μm in size cannot be spatially resolved. The data obtained with this set-up have been calibrated against high-quality fused silica and sapphire absorption standards having absorptions of 10 and 100 ppm/cm respectively.

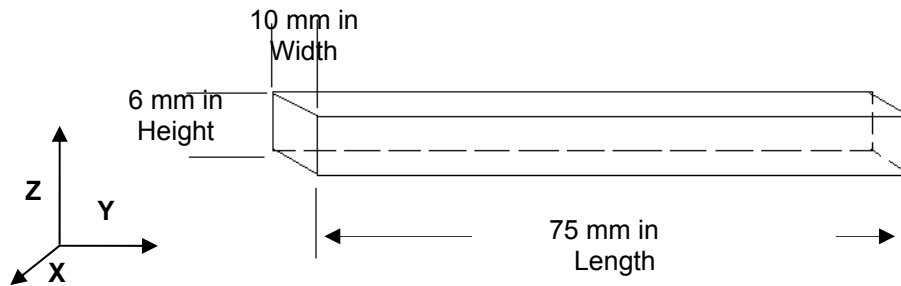


Fig. 17 Configuration of the (PCI) scan measurements on a slab sample

Scans performed through the entire thickness of the three ceramic slabs (Z- direction on Fig. 17) are plotted in Fig.18 and reveal the evolution of the thermalized absorption within the bulk of the samples. All samples have absorption levels on the order of 1000 ppm/cm. These values are comparable to absorption levels that we have measured in the Nd:YAG single-crystal SC1 (Table 2). It is interesting however to note that the Nd and Gd doped samples have significantly higher absorption levels than the undoped ceramic (Table 2). In Fig.18, the peaks appearing on both sides of the samples result from surface absorption and are not accounted for in the average bulk absorption. The small symmetric peaks located outside the Nd-doped sample result from interference of the two laser beams.

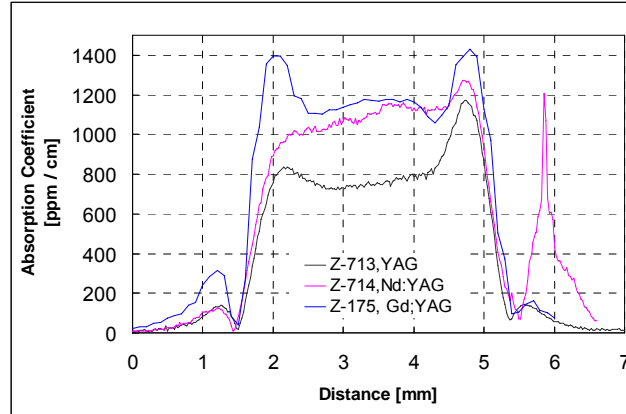


Fig. 18 Thermalized absorption at 1064nm for the Z-713, Z-714 and Z-715 samples

Table 2 Average values of the thermalized absorption coefficients in the investigated samples

	Absorption Coefficient (ppm/cm)
YAG, Z-713	750
Nd:YAG, Z-714	1050
Gd:YAG, Z-715	1100
Single-crystal Sc1	1000
Kono1	135
Fused silica standard	10
Sapphire standard	100

Figure 19 shows two scans performed at constant depth and along the largest dimension of the Nd doped and Gd doped YAG slabs (Y-direction on Fig. 17). In the case of the Gd:YAG sample, sharp spikes occasionally appeared during the scan (Fig. 19a). These spikes were associated with large phase jumps between the two arms of the common-path interferometer and drops in the transmitted pump power. The corresponding features can be unambiguously attributed to light scattering on pores. The size of these pores is estimated to be in the 100-300 μm range. In the Gd:YAG sample, the density of scatters detected by this technique is approximately $1.36 \times 10^5 \text{ cm}^{-3}$ which corresponds to a pore volume fraction of 0.06 ppb. Some larger defects, on the order of 1mm, were also seen in Z-714 (Fig 19b) but at a much lower concentration.

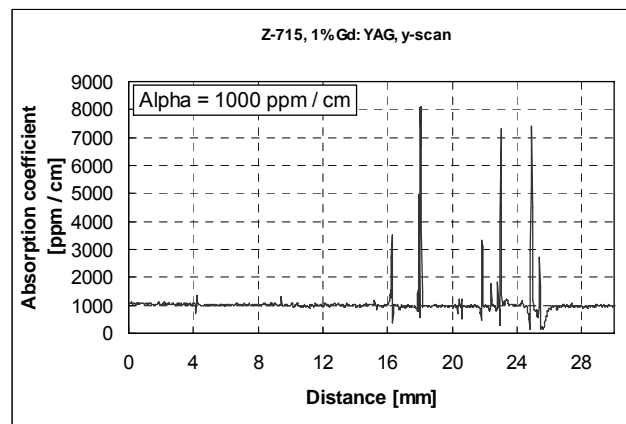


Fig. 19a Thermalized absorption at 1064 nm in Z-715

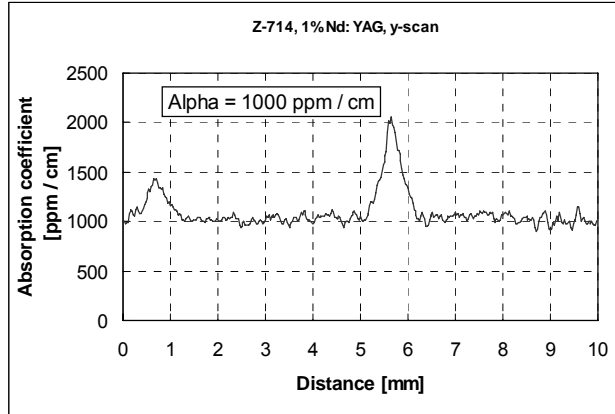


Fig. 19b Thermalized absorption at 1064 nm in Z-714

For comparison, Fig. 20 below shows the absorption profile at 1064nm in the ceramic sample purchased from Konoshima. The average absorption in this material is about seven times lower than in the Z-714 and SC1 samples.

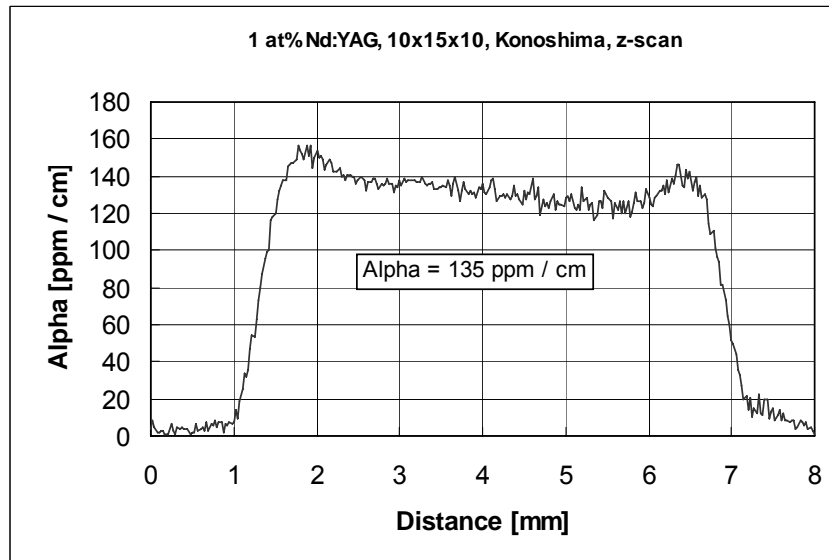


Fig. 20 Thermalized absorption at 1064nm in the 1 at% Nd:YAG produced by Konoshima Corp.

To understand the difference of absorption in different YAG systems, we conducted PCI measurements on 30 YAG samples, both ceramics and single crystals, both doped and undoped. Figure 21 illustrates the absorption coefficients of YAG ceramics and single crystals from different vendors.

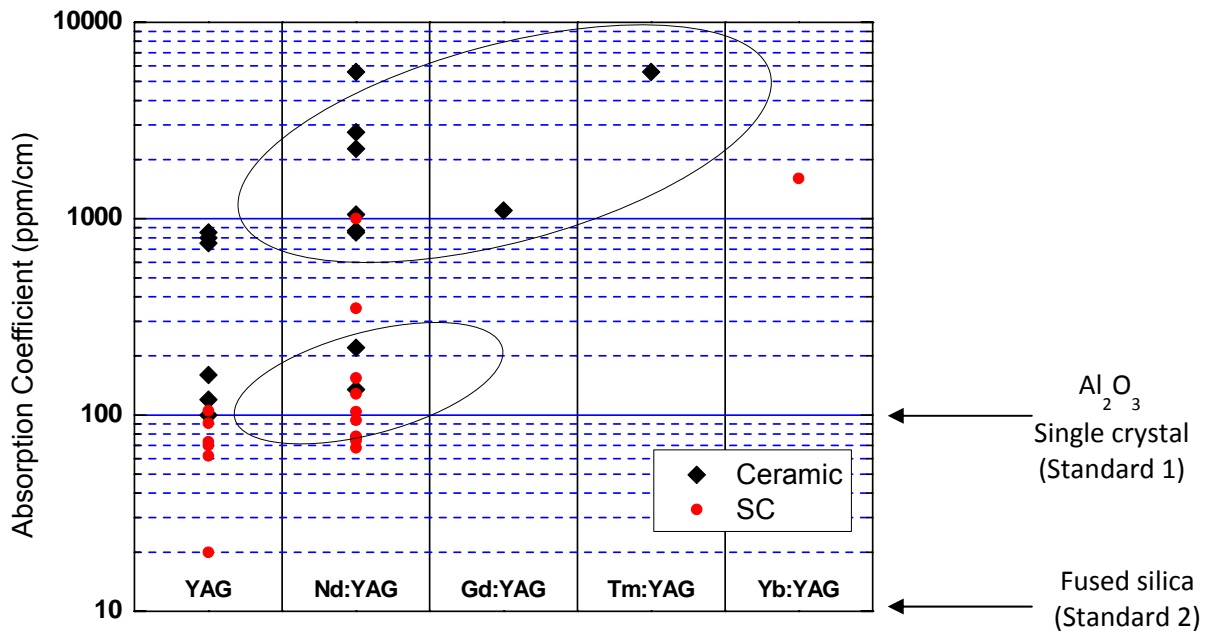


Fig. 21 Absorption coefficient of non-doped YAG and doped YAG ceramics and single crystals at 1064 nm, x-axis indicates different chemical composition. Black and red dots represent ceramics and single crystals, respectively. Top oval includes ceramics (black dots) by reactive sintering, and bottom one includes ceramics by non-reactive sintering.

Figure 21 shows that the absorption coefficient of the various ceramic samples investigated ranged from 100 to 8000 ppm/cm depending on fabrication. It is worth noting that certain ceramic samples have absorption coefficients that rival those of single crystals (~100ppm/cm). From that standpoint, this fact confirms, if it were needed, that high quality ceramics are suitable for high power laser gain media. Figure 21 also suggests that reactively sintered YAG ceramics exhibit, on average, absorption coefficients that are one order of magnitude higher than those measured in non-reactively sintered samples. The fact that higher concentrations of SiO₂ (sintering aid) are typically used in the former process than in the latter has been further investigated as a possible explanation for this observation.

Comprehensive chemical analysis has been performed by Evans Analytical Group (EAG) using inductively coupled plasma mass spec. analysis (ICP-MS) on 25 elements ranging from transition metals, rare earths, alkali, alkaline earths and silicon on a set of selected YAG ceramics and single crystals samples. It was found that, for all samples, the major contaminants were silicon and calcium. The fact that the absorption coefficient in YAG samples correlates with the silicon concentration (and to a lesser extent the calcium concentration) suggests that color centers associated with these ions may contribute to the 1064 nm absorption, as suggested by Fig. 22. Further investigation on defect formation is needed to clarify this phenomenon and help improve the fabrication of low absorption YAG ceramic materials.

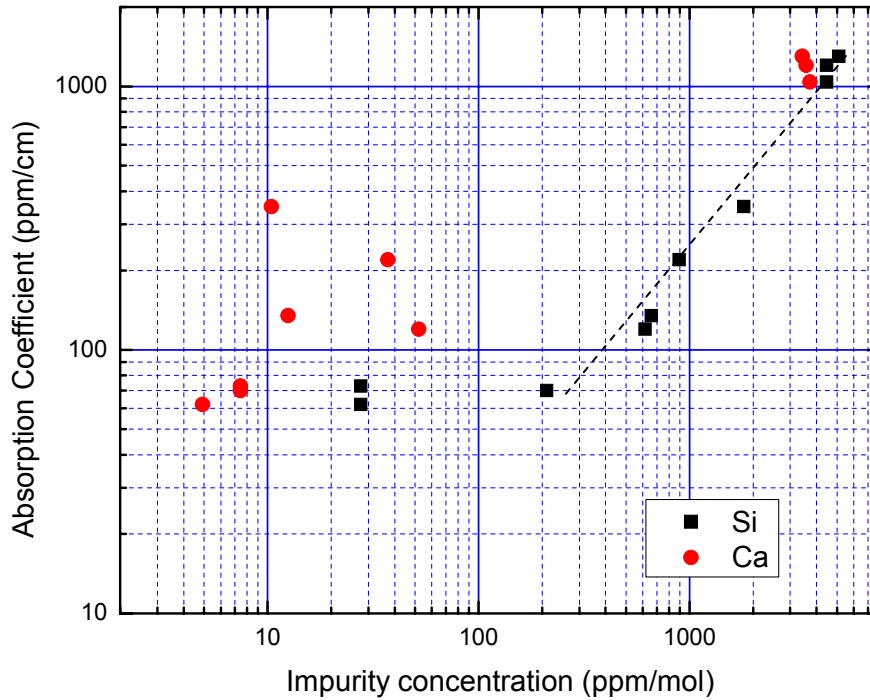


Fig. 22 The concentration of impurity Si^{4+} and Ca^{2+} in different samples with different absorption coefficient (Black squares denote Si^{4+} , and red circles denote Ca^{2+} , dashed line is the linear fit on a log scale.)

2.4.3 Confocal Laser-Gain Scanning Microscopy

We have developed a confocal laser-gain scanning microscope to accurately measure material transmission at a specific laser signal wavelength. This technique simultaneously measures dopant concentration with high-spatial resolution and high dynamic range from ppm levels to several at%. This technique also offers a way to compare quantum efficiency between samples. Optical concentration profilometry can be performed by measuring the absorption or gain of the ion of interest with a resolution limited by the size of the probe and/or pump beams. To achieve high spatial resolution, small spot sizes are required. However, the presence of defects in imperfect transparent ceramics, such as secondary phases and pores, can induce large scattering losses for small spot sizes, which can mask the actual absorbed signal. This problem is mitigated by using a probe beam in addition to the pump beam. If the probe beam is significantly larger than the pump beam, this arrangement reduces the influence of material defects on the final measurement without sacrificing spatial resolution of the reconstructed profile. Figure 23 shows a schematic of a confocal laser-gain scanning microscope.

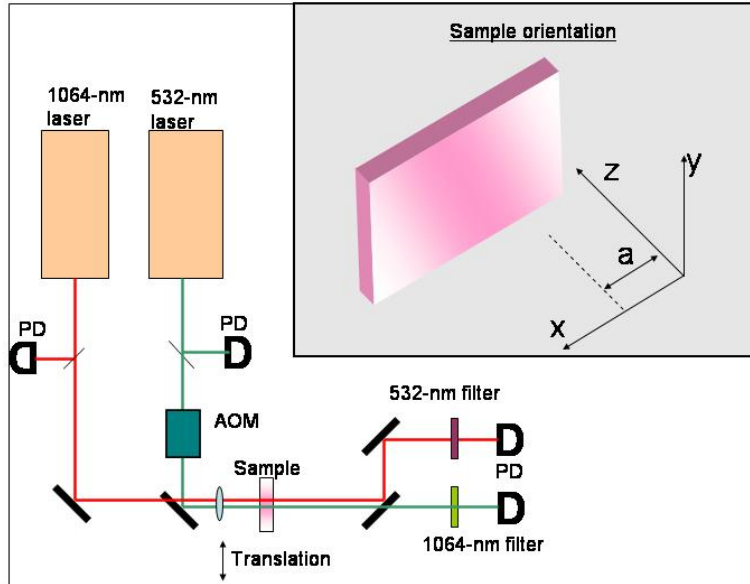


Fig. 23 Experimental setup of the confocal laser-gain scanning microscope for the measurement of doping profiles in transparent YAG ceramics. The sample was translated along the x direction to draw out the profile. The inset shows the orientation of the sample relative to the coordinate axis of the laboratory frame. The laser beams propagate in the z direction, and the profile varies exclusively along the x direction. AOM: Acousto-optic modulator, PD: Photodiode. The probe laser at 1064 nm has a 100 μm beam size and a power of 4 mW. The pump laser at 532 nm has a 250 μm beam size and a power of 1W.

To measure the concentration, the ceramic is optically pumped with a tightly focused laser beam, which excites the REIs contained in the very small pumped volume. A probe beam at a wavelength where the excited REIs exhibit gain is launched into the pumped volume and the extracted power is measured. If bleaching is avoided, the REI concentration can be inferred from this measured extracted power. By scanning the ceramic, it is possible to form one- and two-dimensional images of the concentration profile. The setup for our measurements in Nd^{3+} :YAG consists of an amplitude modulated 532 nm pump beam that is focused into the ceramic. The extracted power at the chopping frequency, f , is monitored with a 1064 nm probe beam which co-propagates with the 532 nm pump. Through suitable selection of the pump and probe wavelengths this technique can be employed for virtually any laser ceramic gain medium.

In this study, 24 mm-long linear scans were performed on the Nd:YAG Z-714 sample with translation increments of 60 or 100 μm . Figure 24 shows the extracted power at 1064 nm in-phase with the modulated pump beam. This extracted power is directly proportional to the concentration of Nd^{3+} ions provided that the quantum efficiency is constant across the sample. Two curves, corresponding to two successive 24mm-scans only overlapping by 2 mm, are represented on this plot. The oscillation of the signal is due to temporal instabilities of the probe diode laser source however the signal fluctuations only represent 0.14% of the signal amplitude. These measurements confirm that sample Z-714 presents a homogenous gain over the entire slab and that both dopant concentration and fluorescence efficiency are uniform.

Scans were also taken at various positions within the width of the sample, at $z = 10, 35$ and 65mm respectively from the top surface of the slab. All these scans are plotted in Fig. 25 and

confirm the overall good uniformity of the gain. On this plot, the slight raise of the gain observed near the edge of the slab (for $z = 65$ mm) is actually an artifact due to the close proximity of the beam and the slab edge. For an intermediate position ($z = 35$ mm), a few spikes of about $100 \mu\text{m}$ width were observed. It was noticed that both pump and probe beams were simultaneously attenuated when passing through these localized regions (Fig. 26). This strongly suggests that these spikes actually correspond to scattering centers. According to our measurements, the density of scatters is on the order of $1.25 \times 10^5 \text{ cm}^{-3}$, which is consistent with the estimate obtained from the thermalized absorption technique.

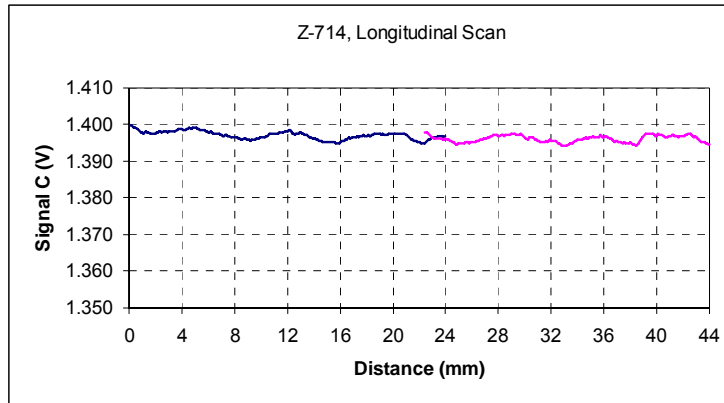


Fig. 24 Scan of sample Z-714 along the Y-axis near the center of the sample.

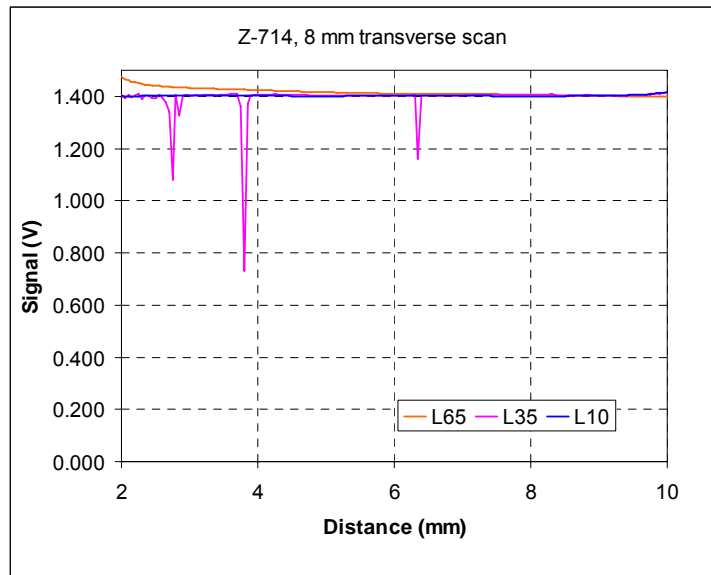


Fig. 25 Scans of sample Z-714 along the X-axis at various z positions relative to the top of the sample ($z = 10, 35, 65$ mm).

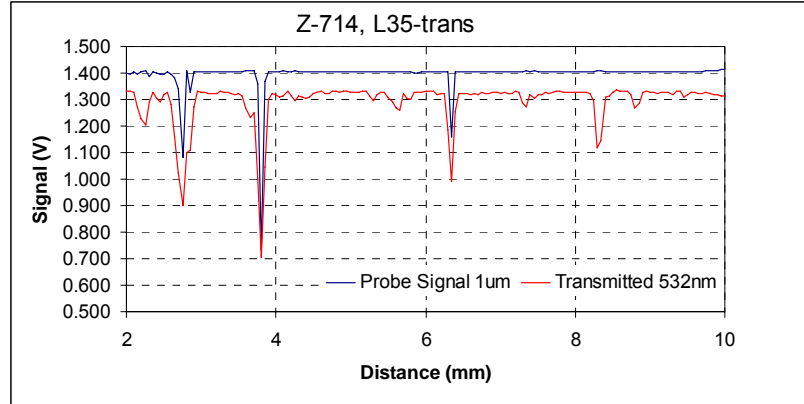


Fig. 26 Details of the scan of sample Z-714 along the X-axis at position $z = 35\text{mm}$

2.4.4 Light Scattering Tomography

Laser scattering tomography (LST) reveals microscopic and submicroscopic particles by elastic scattering of light, in a similar manner that of the old method of ultra-microscopy. Moriya and Ogawa introduced focused laser irradiation and applied this method to characterize a variety of materials [6]. LST uses an intense laser beam with a wavelength in the transparent region of the material under investigation. The beam is focused on the region of interest inside the sample. The illuminated region is imaged at 90° by a microscope, and the distribution of scatters is determined after data processing.

Figure 27 shows our experimental setup. The beam of a He-Ne laser is shaped by a telescope. The light irradiates the scatterers inside the sample, and it is possible to observe 2D LST images. A microscope images the irradiated scatterers onto a CCD camera. The microscope has a low numerical aperture ($NA=0.08$). This low N.A. restricts the resolution to about $10\ \mu\text{m}$. An image processing system is used for frame grabbing and digital integration of the video images. The image processing is then performed by computer. We recently added a vertical and horizontal translation stage covering a 20 mm-range with a precision of $0.1\ \mu\text{m}$ as well as a 360° rotation stage with an angular precision of 0.1° . The rotation stage enables us to observe the shape and the symmetry of scattering defects more clearly. We also implemented LabView VI to control these stages, perform the image capture and process the 2-D image.

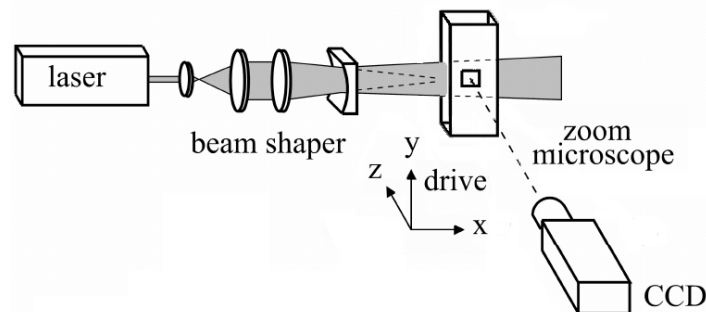


Fig.27 Details of light scattering tomography

LST gives images with high contrast, which can resolve the faintest objects. The defects are observed inside the bulk without damaging the sample. LST is a well-established technique for studies of inclusions (pores or precipitates) and defects decorated by inclusions (such as dislocations). The detectability of defects by this system is dependent upon their scattering power, which depends on the defect physical characteristics such as refractive index difference, piezo-optical birefringence around dislocations and their shapes. The resolving power of this system is better than that of an objective lens because light scattering is caused by much smaller particles and/or refractive index irregularities than the resolving power of the lens, which is very similar to seeing smoke though we cannot recognize particles in the smoke with our eyes. It is a somewhat novel application to adapt LST to measure the size and density of scatters in ceramics. The typical methods for scattering measurement are either measuring scattering loss coefficient over certain length, or using SEM and SAM to identify scatters at the nanoscale. The advantage of LST for ceramic scattering measurement is to provide a bulk view from μm to mm size, as well as more accurate statistical data of scatters' size, density and distribution.

The following pictures (Figs. 28 and 29) show a comparison between the LST images obtained in the five YAG samples studied, all acquisition parameters being equal. The nature of the scattering centers has yet to be determined. Each LST image shown here has been compiled from 50 horizontal translational images, with a step size of $10\mu\text{m}$.

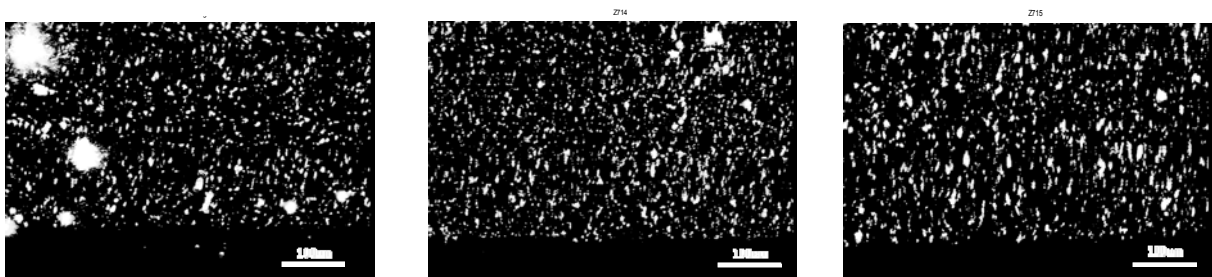


Fig. 28 Comparison of the density of scatters seen by light scattering tomography in sample Z-713 (YAG, left), Z-714 (Nd:YAG, center) and Z-715 (Gd:YAG, right).

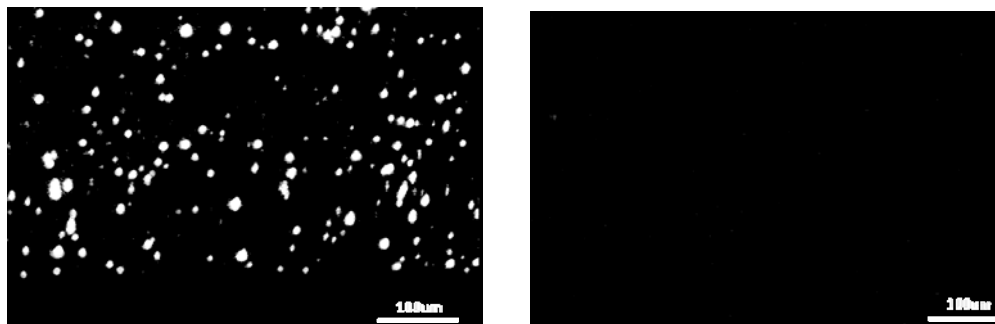


Fig. 29 A comparison of the density of scatters seen by light scattering tomography in a Nd:YAG ceramic sample from Konoshima (Kono1, left) and single-crystal of Nd:YAG (Sc1, right) (The same image acquisition parameters were used as for the images shown in Fig. 28.)

From these pictures, one can estimate the density and the size of the scatters (Table 3). To

confirm the results of LST measurement, the transmittance spectra of Z713 was measured and the Mie model in section 2.2 is used to fit the spectra. The fitting size of scatters is $0.34 \mu\text{m}$ and the number of density is $1.75 \times 10^5 \text{ cm}^{-3}$, which validates the estimate results from LST.

Table 3: Density and size of scatters in the samples investigated by LST

Sample	Z713	Z714	Z715	Kono1	Sc1
Scatter density (cm^{-3})	$8 \cdot 10^4$	$1.1 \cdot 10^5$	$1.04 \cdot 10^5$	$1.5 \cdot 10^3$	Below detection limit
Scatter size (μm)	< 1	< 1	< 1	2~10	Below detection limit

Samples Z-713, Z-714 and Z-715, all made by the reactive sintering method, seem to have on average 10 times smaller scatter sizes than in sample Kono1 made by the non-reactive sintering method. However, the former present up to 100 times more scattering centers than the latter. Results obtained by both LST and thermalized absorption techniques suggest that scattering predominantly occurs from micro-porosity.

In a continuation of this work, we plan to use different laser sources at various wavelengths to better characterize the nature and the size of scatters as well as perform better depth integration and 3-D image processing.

- [6] K. Morea and T. Ogawa, "Observation of growth defects in synthetic quartz crystals by light-scattering tomography" *J. Crystal Growth*, Volume **44**, Issue 1, August 1978, Pages 53-60

2.4.5 Laser Properties

The laser performance of the Nd:YAG sample Z-714 was tested in a simple planar-concave cavity. The sample was pumped at 808 nm by a laser diode, the optics were HR coated at 1064 nm and the end-mirror had a 20 cm radius of curvature (Fig. 30). An anti-reflection coated, 1 at% Nd:YAG single-crystal was also tested under the same conditions for the sake of comparison. The laser performance is plotted in Figs. 31 and 32.

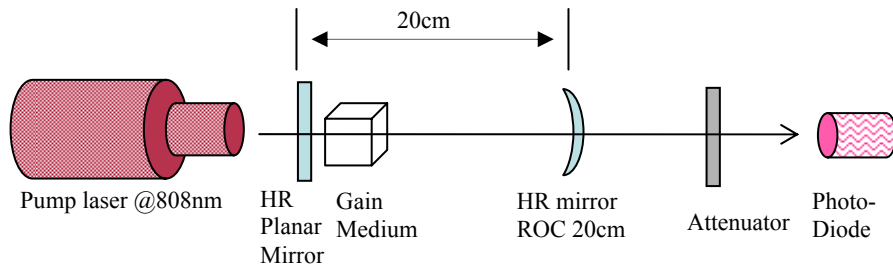


Fig. 30 Schematic of the laser set-up with a planar-concave cavity

The laser threshold for both ceramic and single-crystal is 5.2 W. The optical-optical efficiency of the uncoated ceramic is 9.8 % versus 14.9 % for the AR coated single-crystal.

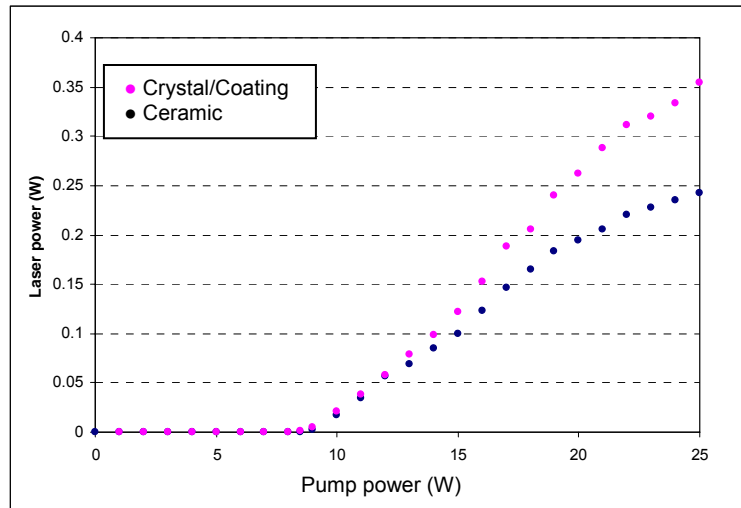


Fig. 31 Laser performance of both Z-714 ceramic and Nd:YAG single crystal Sc1.

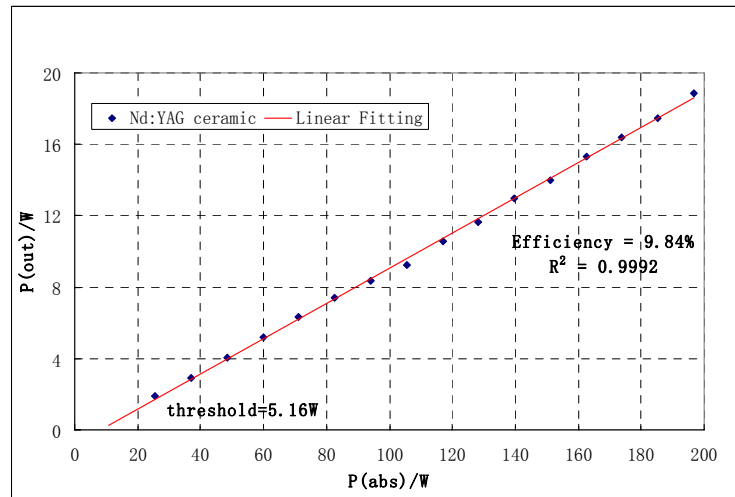


Fig. 32 Calibrated laser efficiency of sample Z-714

III. Directions for Continuing Research

The achievement of stable processing conditions and the recent acquisition of supplemental equipment in our ceramic lab (spray-dryer), help us to control the agglomeration state of the starting powders and make us confident that the optical quality of the ceramics we produce will continue to improve. This will allow us to further study diffusion of dopants and improve the fabrication techniques for laser ceramic composites.

The research described here has also been successful in developing the tools necessary to quantify optical losses in ceramic laser host materials. We have shown a significant correlation between processing variables and optical quality in ceramic materials. Our main goal in future research efforts will be to understand these trends and exploit them to further lower optical losses in ceramic laser host materials. Many questions remain to be answered and will have crucial consequences as far as the fabrication of engineered ceramic gain media is concerned.

IV. Program Participants

Robert L. Byer - Principal Investigator
Romain Gaume - Research Scientist
Roger Route - Senior Research Associate
Ye He - Graduate Student Research Assistant

V. Publications Supported Directly

A.P. Patel, M.R. Levy, R.W. Grimes, R.M. Gaume, R.S. Feigelson, K.J. McClellan, and C.R. Stanek, "Mechanisms of non-stoichiometry in $Y_3Al_5O_{12}$ ", Applied Physics Letters, **93**, 191902 (2008)

J.A. Wisdom, R. Gaume and R.L. Byer, "Laser-gain scanning microscopy: a new imaging technique for engineered laser-gain media", Optics Express, Vol. **18**, Issue 18, pp. 18912-18921 (2010) doi:10.1364/OE.18.018912

J.A. Wisdom, R. M. Gaume, K. Urbanek, T. Plettner, R.L. Byer, A. Guichard, M.Brongersma, A. Kinkhabwala, W.E. Moerner, Akio Ikesue, Yan Lin Aung, "Characterization of a Nd:YAG Ceramic Laser with a 510- μ m-wide Engineered Doping Profile", in preparation.